Rotation–vibration spectra of icosahedral molecules. III. Rotation energy level spectra for halfintegral angular momentum icosahedral molecules

William G. Harter and Tyle C. Reimer

Citation: The Journal of Chemical Physics **94**, 5426 (1991); doi: 10.1063/1.460701
View online: http://dx.doi.org/10.1063/1.460701
View Table of Contents: http://scitation.aip.org/content/aip/journal/jcp/94/8?ver=pdfcov
Published by the AIP Publishing

Rotation–vibration spectra of icosahedral molecules. III. Rotation energy level spectra for half-integral angular momentum icosahedral molecules

William G. Harter and Tyle C. Reimer
Department of Physics, J. William Fulbright College of Arts and Sciences, University of Arkansas, Fayetteville, Arkansas 72701

(Received 20 August 1990; accepted 14 December 1990)

Icosahedral spinor representation theory is developed for analyzing half-integral J eigenlevels of rotational tensor Hamiltonians for molecules such $B_{12}H_{12}^{-2}$, $C_{20}H_{20}$, and C_{60}. Large half-integral J eigenlevels for general sixth rank icosahedral tensors are discussed using different approximations and quantization schemes. Interpretations are made concerning some of the qualitative and semiquantitative spectral structure that is revealed.

I. INTRODUCTION

Mass spectroscopy observations by Curl and Smalley[1] and Kroto[2] of C_{60} clusters has stimulated considerable interest in the possibility of icosahedrally symmetric "Buckminsterfullerene" structures being generated during laser ablation of graphite. There is the related possibility that such highly symmetric ions and molecules occur in carbon-rich stellar nebulae and in some soot producing combustion processes. Recent infrared spectra of carbon dust particles deposited on Ge substrates by Kraetschmer, Fostiropoulos, and Huffman[3(a)] indicated the presence of icosahedrally symmetric C_{60} structures. Subsequently, their claimed observation of macroscopic solid C_{60} has received considerable attention.[3(b),3(c)] Also, the potential exists for spectroscopic studies of other icosahedrally symmetric structure such $C_{20}H_{20}$, which was synthesized by Pacquete *et al.*[4] the borohydride ion $B_{12}H_{12}$ (Ref. 5), and a C_{80} structure recently proposed by Chapman.[6] A recent paper by Ceulemans and Fowler[7] carried out an analysis of Jahn–Teller distortion for the fivefold degenerate state of a neutral icosahedral molecule.

All this has increased our need to understand the spectroscopic consequences of this extraordinary symmetry Y and its representations. (Here we use the conventional notation Y for the group.) The C_{80} structure is particularly intriguing since it is closely related to that of C_{60}; as seen in Fig. 1, both are composed of interlocking pentagons and hexagons. Each carbon in the C_{60} structure sits in an identical environment of C_v symmetry while C_{80} contains twenty "extra" carbon atoms which sit at points of C_{3v} local symmetry.

It is possible that spectroscopic investigation of these highly symmetric cage molecules might first be done using their positive or negative ions, which have lost or gained, respectively, a single electron. The mass spectroscopy[8] which indicates the existence of C_{60}, involves the positive ionic state, and it is well known that many cage molecules form stable negative ions. Recent developments in ion trap technology and ion spectroscopy raise the possibility for identifying and investigating high resolution ionic spectra of these structures. However, the symmetry analysis of singly charged ions is quite different from that of the molecules, which was treated in the preceding articles I and II.[9,10] One must deal with half-integer angular momentum which has very different symmetry properties. For example, the uncoupled half-integer spin of the electron changes sign under a rotation of 2π. This necessitates the use of multiplier or ray representations of the symmetry algebra. Conventional treatments of finite symmetry and crystal field splitting use the faithful representations of the point double groups in the case of half-integral J values. For larger groups, such as the icosahedral group, it helps to reduce computational labor by using a ray algebra,[11,12] in which the operations addition and subtraction are allowed. This has the effect of halving the size of the class algebra rather than doubling it. This symmetry analysis will be useful in analyzing combined spin–orbit-rotation and Jahn–Teller effects in icosahedral molecules with an odd number of electrons.

Nevertheless, there are quite a number of similarities between the symmetry and spectral analysis of half-integral J values and that of integral J values, particularly for the high J limit. In the classical limit the distinction of the two types is diminished. As will be shown here, many of the ap-

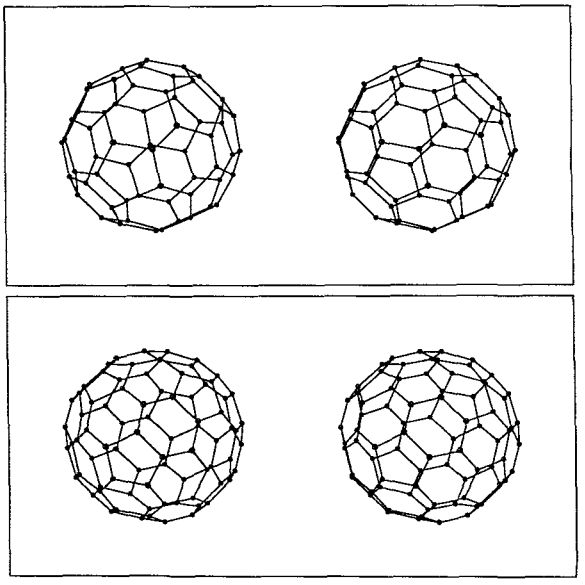

FIG. 1. Stereoscopic views of C_{60} and C_{80}.

 0021-9606/91/085426-09$03.00

proximate semiclassical techniques developed to treat integral spin fine structure in tensor spectra can be applied to half-integral J.

In the past the analysis of ionic nonlinear molecular fundamentals has been well approximated by Hund's Case (b) in which the (integral) rotor momenta N or R were good quantum numbers for nearly degenerate spin doublets. It is not yet known if this applies to C_{60} fundamentals. However, high resolution C_{60} spectroscopy above 50 ° K is likely to require examination of rovibrational overtone structure which may have large N mixing. In any case one should be prepared to handle other Hund's cases and their intermediates which involve half-integral J labeling.

II. FINE STRUCTURE FOR HALF-INTEGRAL J

The icosahedral spectral patterns and analysis are similar but more complex than those seen in laser spectra of octahedral SF_6.[13] Rotational fine structure is modeled by the eigenvalue spectrum of a symmetric tensor operator represented in a $2J+1$ dimensional angular momentum basis. This tensor operator chosen to approximate the icosahedral rotational Hamiltonian is the lowest nonzero rank (nonspherical) irreducible tensor operator having icosahedral symmetry.

$$T^{(6)} = \frac{\sqrt{11}}{5} T^6_0 + \frac{\sqrt{7}}{5}(T^6_5 - T^6_{-5}). \tag{1}$$

This operator will play the same role as Hecht's Hamiltonian did in the octahedral analysis.

To obtain numerical eigenlevels the sixth rank tensor is first represented by a $(2J+1)\times(2J+1)$ matrix in the total angular momentum basis, then numerically diagonalized. The algorithm used to find these eigenvalues is similar to that used in Refs. 9 and 10, with modifications to allow half-integral J, index sorting, and a more precise diagonalization algorithm.[14] High computational precision is needed to resolve the extraordinary level clustering which these high symmetry tensors yield. The $J = 100.5$ case is illustrated in Fig. 2. The bold face letters following each level are icosahedral symmetry species labels for ray representations. E labels twofold degeneracies [There are two kinds labeled by correlations with the SU(2) supergroup, $E_{1/2}$ and $E_{7/2}$ in Table III], G labels fourfold degeneracies, and I labels sixfold degeneracies. None of these should be confused with any of the standard representations A (onefold), T_1 or T_3 (threefold), G (fourfold), or H(fivefold) discussed in Refs. 9 and 10.

It is instructive to view the resultant energy level spectrum with the use of a rotational energy (RE) surface. This surface is a radial plot of the Hamiltonian in terms of the polar, and azimuthal coordinates of the classical J vector as viewed from the body frame of reference. For simplicity, the classical J vector is used to define the lab-fixed z axis. The RE energy is given by

$$\mathrm{RE}(\theta,\phi) = B\,|J|^2 + t_{066}\,T^{(6)}(\theta,\phi), \tag{2}$$

where

$$T^{(6)}(\theta,\phi) = \sqrt{11}\,[231\cos^6\theta - 315\cos^4\theta + 105\cos^2\theta - 5 - 42\cos\theta\sin^5\theta\cos\phi \times(16\cos^4\phi - 20\cos^2\phi + 5)]\,|J|^6/80.$$

The scalar rotational constant is taken to be unity,

$$B\,|J| = 1$$

while the tensor coefficient is chosen as follows to give a clear graphical representation in Fig. 3.

$$t_{066}|J|^6 = 0.2.$$

This surface is similar to the integral case except that quantizing level curves are shifted slightly to approximate half-integer J values. The level curves represent equal-energy level or classical trajectories of the precessing J vector. As seen, the trajectories become more circular in the neighborhood of the stable extrema of the RE surface. The bending of the circular trajectories arises from anisotropic centrifugal distortions the molecule undergoes while rotating. The eigenlevels in Fig. 2 can be related to quantizing level curves on the RE surface. Each set of twelve level curves for a given energy found on the twelve C_5 symmetric peaks corresponds to a 12-fold quasidegenerate cluster. Similarly, each set of

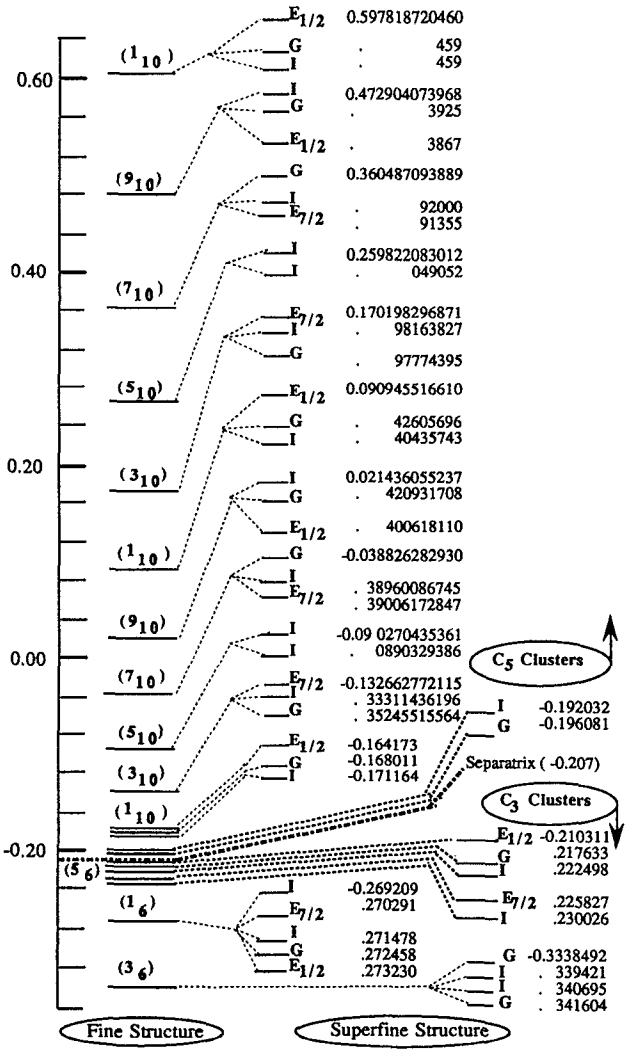

FIG. 2. Eigenvalue spectrum with $J = 100.5$ for sixth-rank tensor Hamiltonian $T^{(6)}$. Superfine-structure splitting are indicated numerically by displaying the significant digits which differ for different species in a cluster. The graphical displays of the splitting are greatly exaggerated.

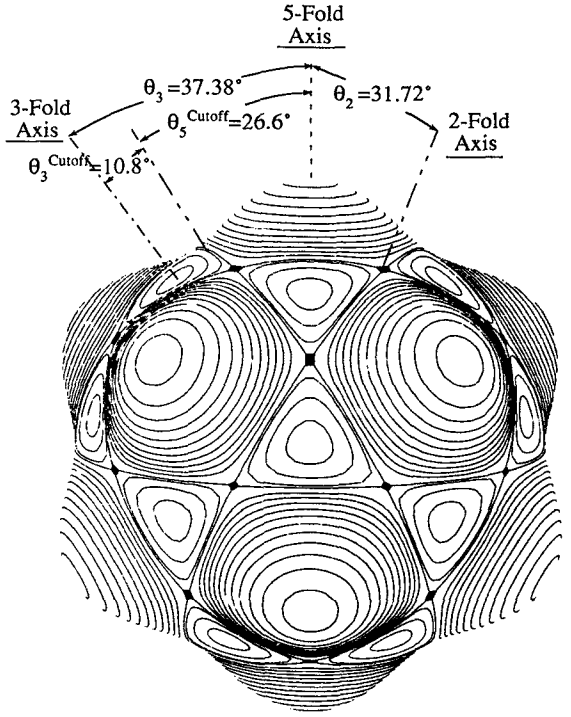

FIG. 3. Rotational energy (RE) surface for the sixth-rank icosahedral tensor Hamiltonian. Quantized trajectories or contours on the 12 fivefold symmetric hills correspond to clusters of 12 levels in Fig. 1, and the quantized contours on the 20 threefold symmetry valleys correspond to the clusters of 20 levels below the separatrix. Angles between key symmetry axes can be used to compute limiting energy values for the two types of clustering. Constants are arbitrarily set to $B,|J|=1.0$, and $t_{066}=0.2$.

twenty levels in the C_3 symmetric valleys corresponds to one of the 20-fold clusters. The separatrix in Fig. 1 consists of great arcs joining the C_2 symmetric saddle points on the RE surface. The polar angles for the C_2, C_3, C_5 axes can be substituted into Eq. (2) to determine bounds for the two types of quasidegenerate clusters. These polar angles were determined to be $\theta_2=31.72°$, $\phi_2=180°$, $\theta_3=37.38°$, $\phi_3=0°$, $\theta_5=0°$, $\phi_5=0°$, where the subscript denotes the local symmetry for that axis. Using Eq. (2), the critical angles have the associated energies,

$$\begin{aligned} \mathrm{RE}(\theta_2,\phi_2) &= -0.207, \\ \mathrm{RE}(\theta_3,\phi_3) &= -0.36, \\ \mathrm{RE}(\theta_5,\phi_5) &= 0.66. \end{aligned} \tag{3}$$

These extreme values do indeed bracket all of the energies in Fig. 1, and as J increases in magnitude the highest cluster approaches the 0.66 limit while the lowest approaches the -0.36 limit. (Table I). Also, the separatrix value accurately locates the energy region in which the 20-fold clusters "melt" into the higher energy 12-fold clusters.

There are several methods that can be used to approximate clusters centroids within each of the bracketed regions. The crudest utilizes a semiclassical approximation, which is an approximation to the first order perturbation correction. The large-J asymptotic limit of the Wigner–Eckart coupling coefficient is used as follows,

$$\left\langle \begin{matrix} J \\ K \end{matrix} \middle| T^r_0 \middle| \begin{matrix} J \\ K \end{matrix} \right\rangle \approx D^r_{00}(.\theta^J_K\cdot)|J|^r = P_r(\cos\theta^J_K)|J|^r \quad (J\gg 1), \tag{4}$$

where θ^J_K is the polar angle of the classical angular momentum J with J_z quantized by K and r is the rank of the tensor operator T. These approximate centroid values and the exact diagonalization values agree to within three significant places for the $J=K=200.5$ case (Table I), with a steady decrease in accuracy for lower K. The first order perturbation, containing only the diagonal terms of the Hamiltonian

TABLE I. Comparison of exact cluster centroids and approximations for C_5 clusters for various half-integral J. Approximation techniques that are used are explained in text.

J	K	Exact values	Cone values	First order	Second order
200.5	200.5	0.629 561 772 569	0.629 144 432 233	0.629 561 744 701	0.629 561 772 569
	199.5	0.563 622 781 797	0.563 232 090 350	0.563 622 609 345	0.563 622 781 793
	198.5	0.500 981 053 974	0.500 615 644 188	0.500 980 430 758	0.500 981 053 947
	197.5	0.441 537 770 448	0.441 195 965 437	0.441 536 052 344	0.441 537 770 322
	196.5	0.385 196 187 831	0.384 875 793 810	0.385 192 186 037	0.385 196 187 350
	195.5	0.331 861 660 933	0.331 559 716 344	0.331 853 391 592	0.331 861 659 355
150.5	150.5	0.618 763 657 744	0.618 031 954 648	0.618 763 567 641	0.618 763 657 742
	149.5	0.532 425 029 442	0.531 755 226 480	0.532 424 465 179	0.532 425 029 407
	148.5	0.451 843 368 808	0.451 231 150 772	0.451 184 302 882	0.451 843 368 565
	147.5	0.376 788 850 427	0.376 228 836 722	0.376 783 073 117	0.376 788 849 207
	146.5	0.307 038 251 391	0.306 523 204 709	0.307 024 582 202	0.307 038 246 440
	145.5	0.242 375 110 328	0.241 894 900 198	0.242 346 364 274	0.242 375 093 002
100.5	100.5	0.597 818 720 5	0.596 217 105 5	0.597 818 242 3	0.597 818 720 4
	99.5	0.472 904 073 9	0.471 502 946 5	0.472 900 997 6	0.472 904 073 1
	98.5	0.360 487 092 5	0.359 264 511 3	0.360 475 477 4	0.360 487 086 0
	97.5	0.259 822 066 0	0.258 749 382 7	0.259 788 411 9	0.259 822 028 7
	96.5	0.170 198 056 2	0.169 233 646 0	0.170 115 064 1	0.170 197 877 8
	95.5	0.090 942 005 9	0.090 021 252 5	0.097 758 592 9	0.090 941 246 3
50.5	50.5	0.539 833 360 5	0.533 922 422 4	0.539 824 403 1	0.539 833 344 6
	49.5	0.315 407 659 7	0.310 901 758 8	0.315 342 968 1	0.315 407 291 2
	48.5	0.136 045 120 0	0.132 549 620 7	0.135 757 802 2	0.136 039 829 6
	47.5	−0.003 325 100 7	−0.006 551 751 7	−0.004 373 015 0	−0.003 363 217 7
	46.5	−0.106 746 534 2	−0.111 405 238 0	−0.110 075 033 9	−0.106 606 239 2
	45.5	−0.200 390 412 6	−0.186 618 012 4	−0.185 976 147 2	−0.171 293 078 4

matrix, can be written in terms of Clebsh–Gordon coefficients.

$$H^{(1)}(K) \approx \frac{\sqrt{11}}{5} t_{066} \left\langle {}^{J}_{K} | T^{6}_{0} | {}^{J}_{K} \right\rangle = \frac{\sqrt{11}}{5} t_{066} C^{6JJ}_{0KK}. \quad (5)$$

This is seen to agree with the exact values to seven significant digits for the $J = K = 200.5$ case. The second order terms containing the Hamiltonian matrix elements that lie five steps off the diagonal give a second order approximation.

$$H^{(2)}(K) \approx H^{(1)}(K) + \frac{|V_5(-K)|^2}{H^{(1)}(K) - H^{(1)}(K+5)} + \frac{|V_5(K)|^2}{H^{(1)}(K) - H^{(1)}(K-5)}. \quad (6)$$

In Eq. (6), as in the entirety of this paper,the reduced matrix element has been set to unity. $H^{(1)}$ is given in Eq. (5), and the V_5 terms are given by the following:

$$V_5(K) = \frac{\sqrt{7}}{5} t_{066} \left\langle {}^{J}_{K-5} | T^{6}_{-5} | {}^{J}_{K} \right\rangle = \frac{\sqrt{7}}{5} t_{066} C^{6JJ}_{-5KK-5},$$
$$\langle J \| 6 \| J \rangle = 1 \quad (7)$$

This approximates the exact values for the centroid of the clusters to within 12 significant digits for the case: $J = 200.5$ and $K = 200.5$. The clusters have the same 12- and 20-fold order of quasidegeneracy that occurred for integer-J levels.[9,10] However, the underlying superfine structure must be different since the ray representations belong to degeneracies of order 2, 4, or 6 instead of 1, 3, 4, or 5.

III. SYMMETRY ANALYSIS OF FINE AND SUPERFINE STRUCTURE

The conventional double group treatment of half integral J would involve double the number of rotational operators in Y and this effectively quadruples the computational labor. Much of this labor can be eliminated by using a group

TABLE II. Class structure of the icosahedral algebra is shown in the highlighted boxes. Class operators are sums over corresponding class elements.

Icosahedral algebra class structure	$\omega = 0°$ $\omega = 360°$	$\omega = 72°$ $\omega = 720 - 72°$	$\omega = 144°$ $\omega = 720 - 144°$	$\omega = 120°$ $\omega = 720 - 120°$	$\omega = 180°$ $\omega = 720 - 180°$
	1+	R1+1	R1+2	r1+1	i1+
	1−	R1−4	R1−3	r1−2	i1−
		R2+1	R2+2	r2+1	i2+
		R2−4	R2−3	r2−2	i2−
		R3+1	R3+2	r3+1	i3+
		R3−4	R3−3	r3−2	i3−
		R4+1	R4+2	r4+1	i4+
		R4−4	R4−3	r4−2	i4−
		R5+1	R5+2	r5+1	i5+
		R5−4	R5−3	r5−2	i5−
		R6+1	R6+2	r6+1	i6+
		R6−4	R6−3	r6−2	i6−
				r7+1	i7+
				r7−2	i7−
				r8+1	i8+
				r8−2	i8−
				r9+1	i9+
				r9−2	i9−
				r10+1	i10+
				r10−2	i10−
					i11+
					i11−
					i12+
					i12−
					i13+
					i13−
					i14+
					i14−
					i15+
					i15−

Class operators

$$C_1 = 1+$$
$$C_R = \sum_{j=1}^{6} (Rj+1) + (Rj-4)$$
$$C_{R'} = \sum_{j=1}^{6} (Rj+2) + (Rj-3)$$
$$C_r = \sum_{j=1}^{10} (rj+1) + (rj-2)$$
$$C_p = 0$$

TABLE III. Correlations between SU(2) angular momentum J states ($J<31/2$) and icosahedral double group species.

J	$E_{1/2}$	$E_{7/2}$	G	I
1/2	1	⋯	⋯	⋯
3/2	⋯	⋯	1	⋯
5/2	⋯	⋯	⋯	1
7/2	⋯	1	⋯	1
9/2	⋯	⋯	1	1
11/2	1	⋯	1	1
13/2	1	1	1	1
15/2	⋯	⋯	1	2
17/2	⋯	1	1	2
19/2	1	1	1	2
21/2	1	⋯	2	2
23/2	1	1	2	2
25/2	1	1	1	3
27/2	⋯	1	2	3
29/2	1	1	2	3

algebra of Y (Refs. 11 and 12) over the complex field as opposed to the Y group. The algebra permits the use of plus and minus operators ($+/-g$) without increasing the dimension of the operator space. The operators will be labeled as follows. Rotations that are multiples of 72° are assigned a upper case "R," rotations that are multiples of 120° labeled by a lower case "r," rotations divisible by 180° are labeled "i," and those divisible by 360° are labeled "1." There are six two sided C_5 axes, corresponding to six rotations R 1,..., R 6, respectively. Similarly, the ten C_3 axes are associated with rotations r1,...,r10, and the fifteen C_2 axial rotations are i1,...,i15. The individual operators are then assigned a plus sign to denote a counter-clockwise rotation of less than 360°, and a minus sign for a clockwise rotation of less than or equal to 360°. A final integer serves as a power or exponent to indicate the number of the fundamental rotations in each operator. For example, $R\,1+3$ is a rotation about the R 1 axis by $3\times72°$ in the counter-clockwise direction. With this formalism, a $R\,1+1$ and its $360+72°$ counterpart $R\,1-1$, differ only by a -1 phase factor $\{R\,1-1=-(R\,1+1)\}$. Then the inverse of $R\,1+1$ is $R\,1-4$. The analysis starts with determining the commutation class operators (Table II), given by the relation,

$$C_h=\sum_{g\in Y} ghg^{-1}. \tag{8}$$

With these class operators, character tables (see Tables IV–VIII) can be constructed as shown in the appendix. The all-commuting projection operators are defined by the relation,

$$P^{\alpha}=\frac{\ell^{\alpha}}{{}^0G}\sum_{C_g}\chi^{\alpha *}_{C_g}C_g, \tag{9}$$

TABLE IV. Icosahedral (Y) ray representation characters.

Y	C_1	C_R	C_{R^2}	C_r
$E_{1/2}$	2	F^+	$-F^-$	1
$E_{7/2}$	2	F^-	$-F^+$	1
G	4	1	-1	-1
I	6	-1	1	0

TABLE V. D_5 ray rep. characters.

D_5	C_1	C_R	C_{R^2}	C_r
A_1	1	-1	1	$-5i$
A_2	1	-1	1	$5i$
E_1	2	F^+	$-F^-$	0
E_2	2	F^-	$-F^+$	0

TABLE VI. C_5 ray rep characters. $\{\zeta_1=\exp(\pi i/5)$ and $\zeta_3=\exp(3\pi i/5)\}$.

C_5	C_1	C_R	C_{R^2}	C_{R^3}	C_{R^4}
$A_{1_{10}}$	1	ζ_1	$-\zeta_3$	ζ_3^*	$-\zeta_1^*$
$A_{3_{10}}$	1	ζ_3	$-\zeta_1^*$	ζ_1	$-\zeta_3^*$
$A_{5_{10}}$	1	-1	1	-1	1
$A_{7_{10}}$	1	ζ_3^*	$-\zeta_1$	ζ_1^*	$-\zeta_3$
$A_{9_{10}}$	1	ζ_1^*	$-\zeta_3^*$	ζ_3	$-\zeta_1$

TABLE VII. Tetrahedral ray rep characters. $\{\zeta_6=\exp(\pi i/3)\}$.

T	C_1	C_r	C_{r^2}
E_1	2	1	-1
E_2	2	$-\zeta_6$	ζ_6^*
E_3	2	$-\zeta_6^*$	ζ_6

TABLE VIII. C_3 ray rep characters. $\{\zeta_6=\exp(\pi i/3)\}$.

C_3	C_1	C_r	C_{r^2}
A_{1_6}	1	ζ_6^*	$-\zeta_6$
A_{3_6}	1	-1	1
A_{5_6}	1	ζ_6	$-\zeta_6^*$

TABLE IX. Correlations between local C_5 cyclic rotational subgroup ray reps and global icosahedral symmetry ray reps.

C_5	$A_{1_{10}}$	$A_{3_{10}}$	$A_{5_{10}}$	$A_{7_{10}}$	$A_{9_{10}}$
$E_{1/2}$	1	0	0	0	1
$E_{7/2}$	0	1	0	1	0
G	1	1	0	1	1
I	1	1	2	1	1

TABLE X. Correlations between local C_3 cyclic rotational subgroup ray reps and global icosahedral symmetry ray reps.

C_3	A_{1_6}	A_{3_6}	A_{5_6}
$E_{1/2}$	1	0	1
$E_{7/2}$	1	0	1
G	1	2	1
I	2	2	2

where the χ are the characters are tabulated, $\ell^{\alpha} = \chi^{\alpha}_{C1}$ is order of degeneracy for α species, and ${}^{0}G = 60$ is the order of the algebra's generating group Y. The characters may be used to find correlations or representations for the subgroup chain $SU(2) \supset Y^{(d)}$ and the symmetry species of their proper subgroups (see Tables III, IX, and X). The procedures for this analysis are given in the appendix.

The correlations for subgroup chains $Y^{(d)} \supset C_5$ (Table IX) and $Y^{(d)} \supset C_3$ (Table X) may be read by columns to indicate which $Y^{(d)}$ symmetry species are contained in a given quasidegenerate cluster of the C_5 and C_3 type. For the $J = 100.5$ levels shown in Fig. 2, the lowest cluster corresponds to $2K = 201 = 3 \bmod 6$ and the 3 mod 6 column of Table VIII which consists of two G and two I species, and these levels appear in the lowest cluster. In the separatrix region the C_3 and C_5 clusters merge and some levels appear to belong to either (or neither) type. However, the ordering remains consistent throughout the entire J manifold as discussed below. The last valid 12-fold degenerate cluster has a minimum or cutoff value which for K can be approximated with use of the angles between the separatrix plane and the C_5 or C_3 axes shown in Fig. 3. The angular momentum cone with this angle corresponds to a cutoff value for the K quantum number.

$$\frac{K^{(5)}_{\text{cutoff}}}{|J|} = \cos(\theta^{(5)}_{\text{cutoff}}). \tag{10}$$

This gives the cutoff values $K^{(5)} = 90.5$ for $J = 100.5$. Similarly, the cutoff angle for the C_3 induced clusters give a cutoff value of $K^{(3)} = 99.5$ for the same total J value.

Level ordering and cluster structure seen in Fig. 2 can be predicted for any half-integral J using Eq. (10) and the wheels shown in Fig. 4. To get the qualitative ordering one need only determine which wheel corresponds to a particular choice of J. This is done by determining which relation $(2J + 1) = 0 \bmod 4$ or $(2J - 1) = 0 \bmod 4$ is satisfied. Next one calculates $2J \bmod 20$ and $2J \bmod 12$ and locates those numbers on the outside and inside of the correct wheel. The level ordering is then found by starting with the correct J value and following the arrows around the wheel until you reach the K-cutoff values calculated by Eq. (10). Taking the $J = 100.5$ case, for example, the bottom wheel applies since J satisfies that wheel's equation $(201 - 1 = 0 \bmod 4)$. The most extreme 12-fold cluster is determined by satisfying $2(100.5) = 1 \bmod 20$. So the highest cluster is a $(E_{1/2}GI)3_{10}$ cluster followed by a $(IGE_{1/2})7_{10}$ cluster, on down to the last complete 12-fold cluster at $K^{(5)} = 90.5$, which satisfies the relation $2(90.5) = 1 \bmod 20$ and corresponds to a 3_{10} cluster $(E_{1/2}GI)$. Similarly, the 20-fold clusters indicated by the inside of the wheel are read off in the opposite direction. These begin with the lowest cluster a 3_6 $(GIIG)$ followed by the cutoff cluster 1_6 $(E_{1/2}GIE_{7/2})$ cluster at $K^{(3)} = 99.5$. The remaining species symbols trapped between these cutoff clusters are those in the neighborhood of the separatrix.

The quantitative spacing of energy levels involves tunneling, one may take the following route used to find the relative intracluster spacing of 12-fold clusters. The tunneling Hamiltonian is parametrized in terms of the tunneling coefficients S between nearest neighbors, T between next-nearest neighbors, O between furthest neighbor, and the diagonal cluster centroid H discussed previously. The states will be labeled in terms of $Y^{(d)}$ rotational operators. These operators are those which take a wave packet of a given local C_5 symmetry and transform this packet over to an equivalent C_5 symmetric neighborhood of the rotational energy surface. The body's z axis is chosen to coincide with the initial state $(|1\rangle)$. The remaining basis states can be identified with left cosets of the C_5 subgroup coincident with the z axis (body). These cosets partition the icosahedral double group into 12 sets, and the action of every operator in a given coset will carry $|1\rangle$ to an equivalent wave packet at the resultant position within a certain phase factor. The induced basis states are taken to be those coset elements (leaders) that maintain similar phase differences between the two local wave packet

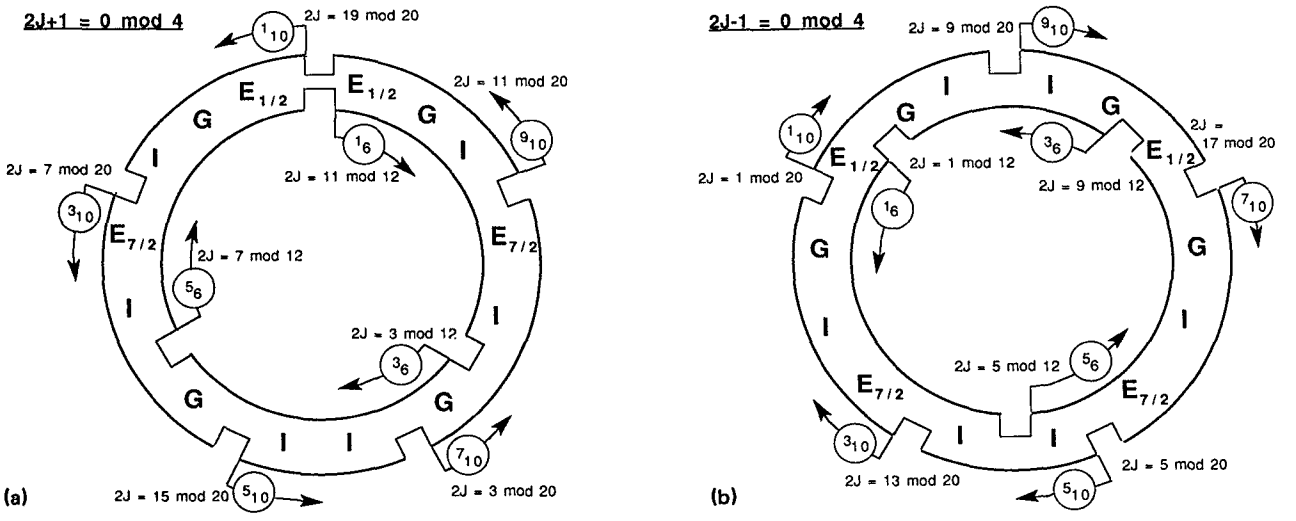

FIG. 4. Sequencing rings of icosahedral symmetry species in sixth-rank tensor spectrum for arbitrary half-integral angular momentum J. Ordering and clustering of species are indicated by segments of the rings as explained in the text.

<H> =

												Labeling of basis states	
H	S	S	S	S	S	T	T	T	T	T	O	|1>	|1+>
S	H	S	T	T	S	S	T	O	T	S	T	|2>	|i1+>
S	S	H	S	T	T	S	S	T	O	T	T	|3>	|i2+>
S	T	S	H	S	T	T	S	S	T	O	T	|4>	|i3+>
S	T	T	S	H	S	O	T	S	S	T	T	|5>	|i4+>
S	S	T	T	S	H	T	O	T	S	S	T	|6>	|i5+>
T	S	S	T	O	T	H	S	T	T	S	S	|7>	|i6+>
T	T	S	S	T	O	S	H	S	T	T	S	|8>	|i7+>
T	O	T	S	S	T	T	S	H	S	T	S	|9>	|i8+>
T	T	O	T	S	S	T	T	S	H	S	S	|10>	|i9+>
T	S	T	O	T	S	S	T	T	S	H	S	|11>	|i10+>
O	T	T	T	T	T	S	S	S	S	S	H	|12>	|i11+>

FIG. 5. Representation of the C_5 induced tunneling Hamiltonian for a particular choice of coset leaders. The tunneling coefficients H, S, T, and O contain $\sqrt{-1} = i$ phase terms introduced by this choice of coset leaders.

states. Figure 5 shows the representation of the tunneling Hamiltonian in a basis consisting of coset leaders that are 180° rotations. This choice of leaders introduce a phase factor of $\sqrt{-1} = i$ in the S, T, and O tunneling parameters. The reduced tunneling matrix elements may then be found using symmetry projection algebra,

$$\begin{aligned}\left\langle {}^{\alpha}_{mn}|H|{}^{\alpha}_{pq}\right\rangle &= \langle 1|P^{\alpha}_{nm}HP^{\alpha}_{pq}|1\rangle/N^{\alpha}\\ &= \langle 1|HP^{\alpha}_{nq}|1\rangle\delta_{mp}/N^{\alpha}\\ &= \frac{\ell^{\alpha}}{{}^{0}G}\sum_{g}\langle 1|Hg|1\rangle D^{\alpha *}_{nq}(g)\delta_{mp}/N^{\alpha}\\ &= \frac{\ell^{\alpha 0}H}{{}^{0}G}\sum_{h}\langle 1|H|h\rangle D^{\alpha *}_{nq}(h)\delta_{mp}/N^{\alpha}\\ &= \sum_{h}\langle 1|H|h\rangle D^{\alpha *}_{nq}(h)\delta_{mp}. \end{aligned} \tag{11}$$

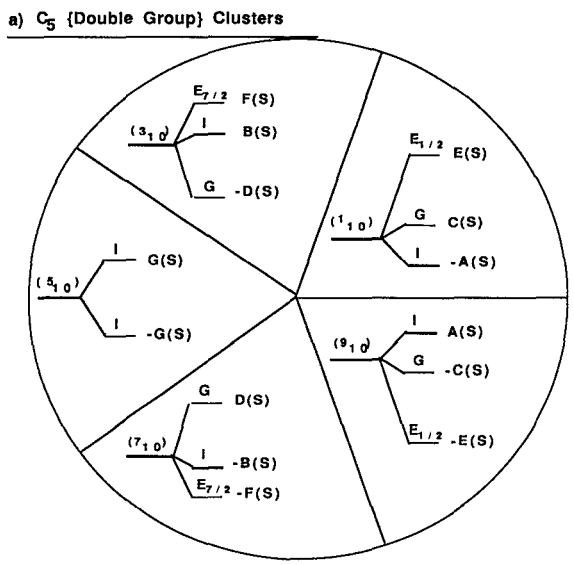

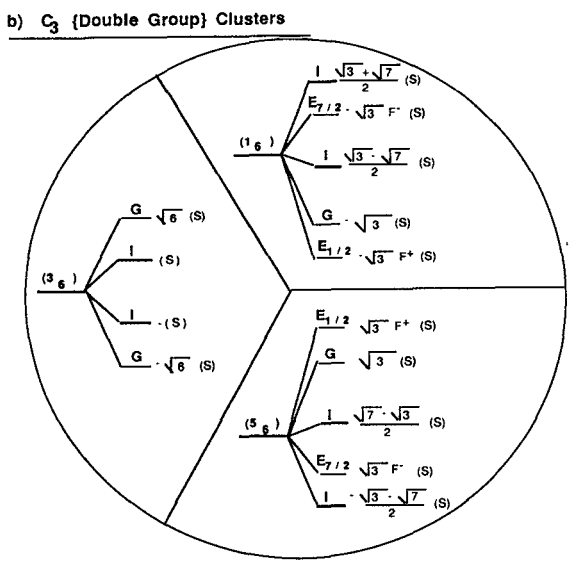

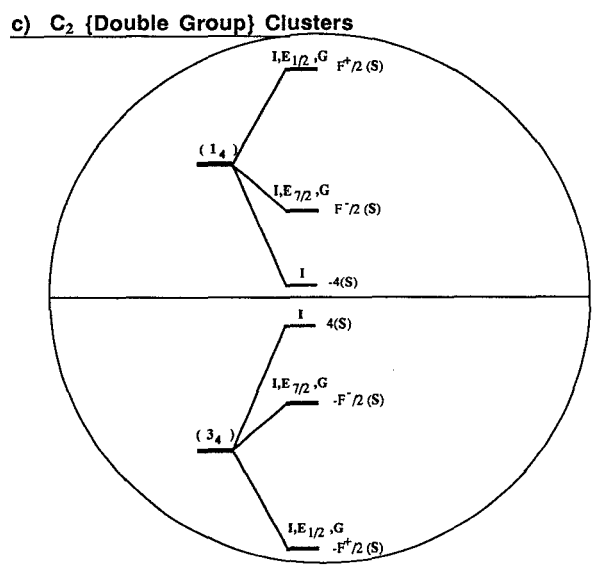

FIG. 6. Detailed form of superfine structure for associated with three types of local symmetry. Level splittings fo reach of the symmetry species are given relative to the cluster centroid in terms of its nearest-neighbor tunneling amplitude S. Note that those clusters grouped one above the other are inverted with respect to each other: (a) C_5 local symmetry, (b) C_3 local symmetry, (c) C_2 local symmetry. Numerical key: $A = (2+F^{+})^{1/2} = 1.902\,12$, $B = (2+F^{-})^{1/2} = 1.175\,57$, $C = (7-4F^{+})^{1/2} = 0.726\,54$, $D = (7-4F^{-})^{1/2} = 3.077\,69$, $E = (10+5F^{+})^{1/2} = 4.253\,25$, $F = (15-5F^{+})^{1/2} = 2.628\,66$, $G = (5)^{1/2} = 2.236\,06$, $F^{+} = (1+5^{1/2})/2 = 1.618\,034$, $F^{-} = (1-5^{1/2})/2 = -0.618\,034$, (S)–Nearest-neighbor tunneling coefficient.

TABLE XI. Comparisons of intracluster superfine splittings. Note that some of the J values are different and that some ratios were taken as the reciprocal of the conjugate cluster ratio (see Fig. 5).

C_5	Induced representation	Accurate numerical values			
		$J=50.5$	$J=100.5$	$J=150.5$	$J=200.5$
$\frac{E_{7/2}-1}{I-G}=$	0.341 641	0.332...	0.341 638	0.341 642	0.341 641
$\frac{E_{1/2}G}{G-I}=$	1.341 642	1.341 563	1.341 635	1.341 641	1.341 641
C_3		$J=48.5$	$J=100.5$	$J=150.5$	$J=200.5$
$\frac{(G+)-(I+)}{(I+)-(I-)}=$	0.724 744	1.034[a]	0.729 537	0.724 947[b]	0.724 870
$\frac{(I+)-E_{7/2}}{E_{7/2}-(I-)}=$	0.732 29	1.149...	0.912 585	0.732 668	0.732 29[c]
$\frac{E_{7/2}-(I-)}{(I-)-G}=$	1.197 71	1.222...	1.210 003	1.197 907	1.197 69[c]
$\frac{(I-)-G}{G-E_{1/2}}=$	1.191 27	1.337...	1.269 764	1.191 560	1.191 25[c]

[a] $J=49.5$.
[b] $J=148.5$.
[c] Determined from reciprocal of conjugate cluster ratio.

Here the summation is over the coset leaders. Only the first row of the original tunneling Hamiltonian matrix is needed. The results for the case where the T and O are assumed to be negligible ($T=O=0$) are shown in Fig. 6(a).The 20-fold clusters determined in the same manner are shown in Fig. 6(b). One notices that the 1_{10} and the 9_{10} clusters are additive inverses of each other, and the same holds for the 3_{10} and 7_{10}, as well as the 1_6 and 5_6 clusters.

It is instructive to compare the ratios of adjacent energy spacing of the exact values with those found by induced representations. These ratios are tabulated in Table XI for several J values and both the 12-fold and 20-fold clusters. The comparison improves with increasing J, since the more isolated wave packet is influenced predominantly by its nearest tunneling opportunity. The same holds for 12-fold clusters which can become even more isolated than their 20-fold counterparts as seen in Fig. 2, because of the larger phase space angle separating the axes of the C_5 symmetric peaks.

IV. CONCLUSION

Semiclassical and graphical methods have been applied in approximating and visualizing rotational eigensolutions of icosahedrally symmetric molecules having nonzero spin. These methods provide simple ways to analyze the eigenvectors and eigenvalues of a variety of tensor Hamiltonians having icosahedral symmetry. Methods were presented to predict the forms and patterns of fine structure that might arise in laser spectra of ionized molecule suitably described by icosahedral tensor Hamiltonians.

ACKNOWLEDGMENTS

This work is supported by Grant No. CHM 89-16787 from the National Science Foundation. We would also like to thank D. E. Weeks for his help and encouragement in getting this paper started.

APPENDIX: IRREDUCIBLE REPRESENTATIONS, CHARACTERS, AND CORRELATIONS

To begin the analysis one must be able to produce the irreducible representations of each rotation operator for every icosahedral symmetry species α. One way to determine these irreps is by subduction from the SU(2) supergroup (or algebra). The standard formula (Ref. 15) for these irreps in any J total angular momentum basis given the Euler angles (α,β,γ) of the rotational operator.

$$D^j_{mn}(R(\alpha,\beta,\gamma))=\sum_{k=0}(-1)^k\frac{\sqrt{(j+m)!(j-m)!(j+n)!(j-n)!}}{(j+m-k)!k!(j-n-k)!(n-m+k)!}\times e^{-i(m\alpha+n\gamma)}(\cos(\beta/2))^{2j+m-n-2k}(\sin(\beta/2))^{n-m+2k}. \quad \text{(A1)}$$

The SU(2) representation is irreducible and unitary:

$$D^j_{mn}(R^{-1}(\alpha,\beta,\gamma)) = D^{j*}_{nm}(R(\alpha,\beta,\gamma)). \quad \text{(A2)}$$

The frequency of occurrences of an icosahedral symmetry species α, arising via subduction from the J representation, can be found using standard character analysis.

$$f^\alpha = \frac{\ell}{{}^0G}\sum_{C_g}\chi^{\alpha *}_{C_g}({}^0C_g)\mathrm{Tr}(D^j(g)). \quad \text{(A3)}$$

Here the irreducible characters are

$$\chi^\alpha_{C_g} = \mathrm{Tr}(D^\alpha_{ij}(g))$$

and g is a representative of each commutation class,and ${}^0C_g$ is the number of operators in that class. The SU(2) characters for the icosahedral classes depend only on their angle (ω) of rotation for each class element and upon the total angular momentum j:

$$\chi^\alpha_{C_g} = \mathrm{Tr}(D^j(R(\omega,0,0))) = \frac{\sin((j+1/2)\omega)}{\sin(\omega/2)}. \quad \text{(A4)}$$

The correlations found using Eqs. (A3) and (A4) are presented in Table III. One notices, that the SU(2) characters for $j = 1/2,3/2$, and $5/2$ correlate with the icosahedral characters $E_{1/2}$,G, and I, respectively. This also implies that the representations also map in a similar manner. The remaining doubly degenerate $E_{7/2}$ is seen to correlate with the $D^{7/2}$ irrep only when taken as a direct sum with the I species, and therefore must be determined by a different method.

This method involves finding the corresponding $E_{7/2}$ projection operators ($P_i^{E7/2}$), and using the relation,

$$P^\alpha_i g P^\beta_j = D^\alpha_{ij}(g)P^\alpha_{ij}\delta_{\alpha\beta}. \quad \text{(A5)}$$

One starts by choosing an Abelian subgroup, for example C_5, and a proper chain of subgroups connecting it with Y, $Y \subset D_5 \subset C_5$, for example.The complete set of all-commuting projection operators is found for each group in the chain using

$$P^\alpha = \frac{\ell^\alpha}{{}^0G}\sum_{C_g}\chi^{\alpha *}_{C_g}C_g \quad \text{(A6)}$$

with C_g being the sum of elements in the class that contains g. Since the P^α are complete in each group algebra, we have the following relation:

$$\sum_\alpha P^\alpha = 1. \quad \text{(A7)}$$

If α denotes the icosahedral species, δ denotes the D_5 species, and σ the C_5 labels, then the nonzero terms in the product

$$\left(\sum_\alpha P^\alpha\right)\left(\sum_\delta P^\delta\right)\left(\sum_\sigma P^\sigma\right) = 1 \quad \text{(A8)}$$

give the idempotent projection operators in Eq. (A5). Two of these will be the $E_{7/2}$ projectors,which will be labeled as $P_1^{E_{7/2}}$ and $P_2^{E_{7/2}}$. The method used earlier [Eqs. (A3)] can be used to find correlation Tables III–IX. These results indicate the useful projection product in the expansion of Eq. (A8) which deliver the $P^{E_{7/2}}$ idempotents. Starting with Table V, the $E_{7/2}$ row correlates with the $A_{3 \bmod 10}$ and $A_{7 \bmod 10}C_5$ symmetry species, which in turn correlate with the D_5 species E_2 ending with the $P^{E_{7/2}}$ icosahedral all-commuting projector. This leads to

$$P_1^{E_{7/2}} = P^{E_{7/2}}P^{E_2}P^{A_{3 \bmod 10}},$$
$$P_2^{E_{7/2}} = P^{E_{7/2}}P^{E_2}P^{A_{7 \bmod 10}}. \quad \text{(A9)}$$

Products of the normalized projection operators in Eq. (A9) (Normalized operators are denoted with a hat.) give the idempotents and nilpotents,

$$\hat{P}_i^{E_{7/2}}\hat{P}_j^{E_{7/2}} = \hat{P}_{ij}^{E_{7/2}}. \quad \text{(A10)}$$

The representation matrix is determined by

$$\langle \hat{P}^\alpha_{ij}|g|\hat{P}^\beta_{kl}\rangle = D^\alpha_{ik}(g)\delta^{\alpha\beta}\delta_{jl}. \quad \text{(A11)}$$

From Eq. (22) it follows that

$$g|\hat{P}^\beta_{kl}\rangle = \sum_i D^\alpha_{ik}(g)|\hat{P}^\beta_{il}\rangle \quad \text{(A12)}$$

and one need only to make the appropriate choice of indices to determine the components of $D^\alpha(g)$. For example, to determine the $D^{E_{7/2}}_{12}(g)$ component, set $k = 2$ and $l = 1$ to arrive at

$$g|\hat{P}^{E_{7/2}}_{21}\rangle = D^{E_{7/2}}_{12}(g)|\hat{P}^{E_{7/2}}_{11}\rangle + D^{E_{7/2}}_{22}(g)|\hat{P}^{E_{7/2}}_{21}\rangle. \quad \text{(A13)}$$

The desired matrix component is found to be

$$\langle \hat{P}^{E_{7/2}}_{11}|g|\hat{P}^{E_{7/2}}_{21}\rangle = D^{E_{7/2}}_{12}(g). \quad \text{(A14)}$$

Notice that the action of g as an operator mixes only those projected states that share the same local symmetry, which is denoted by the second subindex.

[1] R. F. Curl and R. E. Smalley, Science **242**, 1139 (1988).
[2] H. W. Kroto, Nature **329**, No. 6139, 529 (1987).
[3] (a)W. Kraetschmer, K. Fostiropoulos, and D. R. Huffman, Chem. Phys. Lett. **170**, 167 (1990); (b) W. Kraetschmer, Lowell D. Lamb, K. Fostiropoulos, and D. R. Huffman, Nature **347**, 354 (1990); Science **250**, 209 (1990); (c) G. Meijes and D. S. Bethune, J. Chem. Phys. **93**, 7800 (1990); Chem. Phys. Lett. **175**, 1 (1990).
[4] L. A. Paquette, R. J. Ternasky, D. W. Balough, and G. Kentgas, J. Am. Chem. Soc. **105**, 5446 (1983).
[5] C. L. Beckel and James P. Vaughan, in *Boron-Rich Solids*, edited by D. Emin, T. Aselage, C. L. Beckel, I. A. Howard, and C. Wood (AIP Conf. Proc. No. 140) (AIP, New York, 1985); J. A. Wunderlich and W. N. Lipscomb, J. Am. Chem. Soc. **82**, 4427 (1960).
[6] O. L. Chapman and I. Amato, *Making Chicken Wire of Molecular Size*, Science News, **136**, (1990).
[7] A. Ceulemans and P. W. Fowler, J. Chem. Phys. **93**, 1221 (1990).
[8] H. W. Kroto, Science **242**, 1139 (1988).
[9] W. G. Harter and D. E. Weeks, J. Chem. Phys. **90**, 4727 (1989).
[10] D. E. Weeks and W. G. Harter, J. Chem. Phys. **90**, 4744 (1989).
[11] W. G. Harter, J. Math. Phys. **10**, 739 (1969).
[12] W. G. Harter and N. dos Santos, Am. J. Phys. **46**, 251, 264 (1978).
[13] K. C. Kim, W. B. Person, D. Seitz, and B. J. Krohn, J. Mol. Spectrosc. **76**, 332 (1979).
[14] W. H. Press, B. P. Flannery, S. A. Tenkolsky, and W. T. Vetterling, *Numerical Recipes* (Cambridge University, Cambridge, 1986).
[15] L. C. Biedenharn and J. D. Louck, in *Encyclopedia of Mathematics and its Applications, 8. Angular Momentum in Quantum Physics*, edited by G. Rota (Addison Wesley, New York, 1981), pp. 46–55.